Design and Calibration of a Microfabricated 6-Axis Force-Torque Sensor for Microrobotic Applications

F. Beyeler, *Member, IEEE*, S. Muntwyler, and B.J. Nelson, *Member, IEEE*

Abstract—**This work describes the design of a capacitive multi-axis force-torque sensor for the monitoring of forces in the sub-milli-Newton and sub-micro-Newtonmeter range. This force range makes it a valuable tool for microrobotic applications. The sensor is experimentally investigated and calibrated. This is the first microfabricated 6-axis force-torque sensor that has been successfully developed.**

I. INTRODUCTION

F ORCE sensing is an important objective for micro- and nanorobotics [1,2]. In order to avoid damaging objects during the manipulation process, force feedback is important for a reliable functionality. Especially for the automated handling and characterization of biological samples such as single cells and embryos, force feedback is required [3]. The forces dominating micromanipulation are in the range of tens of nano-Newton (10^{-9}N) up to hundreds of micro-Newtons (10^{-6}N) [1,4]. The most common techniques used for force sensing in this range are that of atomic force microscopy (AFM) or piezoresistive cantilevers. Capacitive force sensing probes are also recently available as commercial products [5]. With these force sensing systems, forces along a single axis or two axes can only be measured. For some applications such as automated cell injection, multi-axis force feedback is advantageous, since a misalignment between the injection pipette and the cell can be detected [6]. Other areas such as material characterization and microsurgery [7] also require multi-axis sensors.

In large-scale robotics, six-axis force-torque sensors are state-of-the-art, providing the complete force and torque information on the end-effector. Conventional high-precision six-axis force-torque sensors such as the ATI Nano17 feature a resolution of 3.1mN and 15.6mNm. This is about three orders of magnitude too high for the application fields mentioned above. A six-axis force-torque sensor operating in the range of micro-Newtons can provide a valuable and versatile tool for many micromanipulation tasks.

Recently, three-axis piezoresistive force sensors have

been described [8, 9, 10, 11]. These sensors are designed for measuring forces up to a single Newton. In [3] a high resolution three-axis force sensor for bio-micromanipulation is presented. Little work exists on MEMS torque measuring devices. A piezoresisitve MEMS torque sensor has been described in [12]. In [13] two force components and one torque component have been measured for the characterization of magnetic material properties.

A multi-axis sensor based on magnetic springs has been presented in [14].

This work presents the design of the first micro-fabricated six-axis force/torque sensor. The sensing principle is based on the measurement of a deflection of the sensing element by a number of variable capacitors. The fabrication process is described which was used to manufacture sensor prototypes. Additionally, the calibration of the six-axis device is presented.

II. SENSOR DESIGN AND WORKING PRINCIPLE

The force-torque sensor consists of three main parts:
- A movable body (including a probe overhanging the rest of the device) on which the load is applied.
- An elastic structure which converts the load into a translation and a rotation of the movable body.
- A total of seven variable capacitors which sense the position of the movable body at different positions.

Fig. 1 shows a photograph of the six axis sensor. The dimensions of the device including the probe are 10mm x 9mm x 0.5mm. The movable body, the capacitors and the flexures are made of bulk silicon.
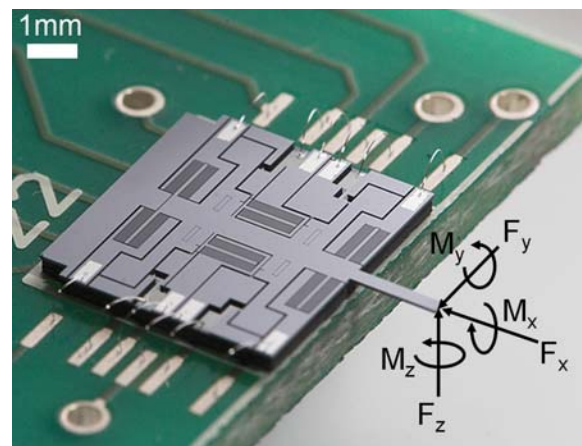

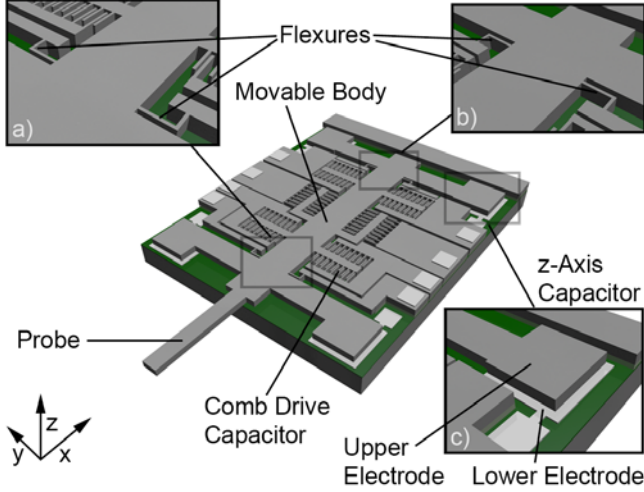Fig. 1. Photograph of the six-axis force-torque sensor prototype.

Fig. 2. Sensor schematics (solid model)

The schematics in Fig. 2 illustrate the movable body of the MEMS sensor as well as the position of the elastic flexures and the capacitors for position sensing. The four flexures allow the movable body to translate and rotate along the x-, y- and z-direction.

The variable capacitors are designed such that they are sensitive in a single direction only. The x-capacitors sense displacements in x-direction, the y-capacitors displacements in y-direction and the z-direction displacements in z-direction. All capacitors sense displacements by transverse motion, which means that a high sensitivity can be obtained for all axes [15]. Also, making use of transverse capacitors enables the design of stiffer sensors while maintaining a high resolution. A high stiffness is desired for high bandwidth measurements.

Fig 3. illustrates the geometry of the capacitors. The x-capacitors as well as the y-capacitors are comb drives to increase the overlapping area of the capacitor as show in Fig. 3a). The z-capacitors shown in Fig. 3b) consist of two square electrodes with a thin air gap in between. Table I gives the numerical values for the geometry of the capacitors as well as the zero-load capacitance. The device layer thickness of the wafer is t; n is the number of capacitor plate pairs of a comb drive; $Cx= Cy$ the capacitance of the comb drives; and Cz the capacitance of the z-capacitor.
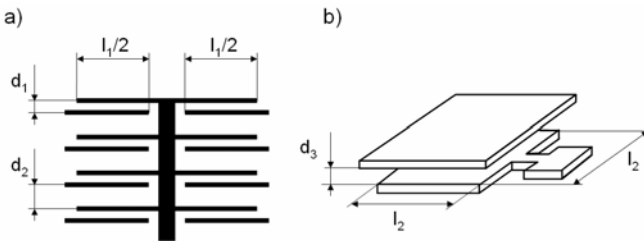

Fig. 3. Geometry of the displacement sensing capacitors

x-axis and y-axis capacitor (comb drive)		z-axis capacitors	
d_1,d_2	5μm, 2μm	d_3	5μm
t	100μm		
l_1	260μm	l_2	1000μm
n	30		
$C_x =C_y$	1.84pF	C_z	1.78pF

Fig. 4 shows the deflection of the movable body when a load component is applied to the sensor probe. The plus-sign and the minus-sign indicate whether the capacitance increases or decreases due to a positive force or torque component. The capacitor pair C_1, consisting of C_{1a} and C_{1b}, is used to measure deflections in the x-direction caused by F_x. By measuring the difference of two capacitors instead of absolute capacitance it is possible to compensate for unwanted disturbances. The differential configuration also creates a linear relationship between deflection and the sensor output signals for small deflections [15]. Since the comb drive pair is only sensitive in the x-direction, this capacitor pair is also called the x-capacitor. For measuring deflections in the y-direction caused by F_y and M_z, the two y-capacitors C_2 and C_3 are used. Again, C_2 and C_3 consist of C_{2a}, C_{2b} and C_{2a}, C_{2b}, respectively, for differential measurements. The force component F_z as well as the torque components M_x and M_y cause a deflection in the z-direction. This deflection is sensed at four positions using the z-capacitors C_4, C_5, C_6 and C_7.

In Figure 4 a coupling between F_y and M_z can be seen. Also, there is a strong coupling between F_z, M_x and M_y. However, due to the placement of the flexures and capacitors the ratio of the signals is not identical for different load components so all six force-torque components can be decomposed. Mathematically, the relationship between the measured deflections $d=[d_0,…,d_7]^T$ and the load $F=[F_x, F_y, F_z, M_x, M_y, M_z]^T$ applied to the probe of the sensor is given by the stiffness matrix $\underline{K}$.

$$
\begin{bmatrix} F_x \\ F_y \\ F_z \\ M_x \\ M_y \\ M_z \end{bmatrix} = \underline{\underline{K}}^{6x7} \cdot \begin{bmatrix} d_1 \\ d_2 \\ d_3 \\ d_4 \\ d_5 \\ d_6 \\ d_7 \end{bmatrix} \tag{1}
$$

This notation assumes a linear relationship between the applied load and the deflection. For the given design the deflections are in the range of a micron which is on the order of 1% of the total flexure length, thus satisfying linearity assumptions.

The calibration matrix $\underline{K}$ includes the mechanical stiffness of the device and the mechanical crosstalk between the axes. To be able to decompose the force and torque components, $\underline{K}$ must have full rank. The condition number of $\underline{K}$ is a

measure for the quality of the sensor design. A small numerical condition number results in a good decomposability. During the design phase simulations have been performed to optimize the placement of the capacitors and to obtain a suitable flexure design which results in a similar sensitivity along the different axes. The design with the smallest condition number $\underline{K}$ was fabricated. Simulations also show that the lowest resonance frequency which limits the bandwidth of the of the sensor is 2.2kHz.

The proposed design performs a deflection measurement at seven positions. For a full six-axis force sensor six position measurement would be sufficient, therefore one of the z-axis measurements is redundant. Four z-axis capacitors are included in the design to improve decomposability.
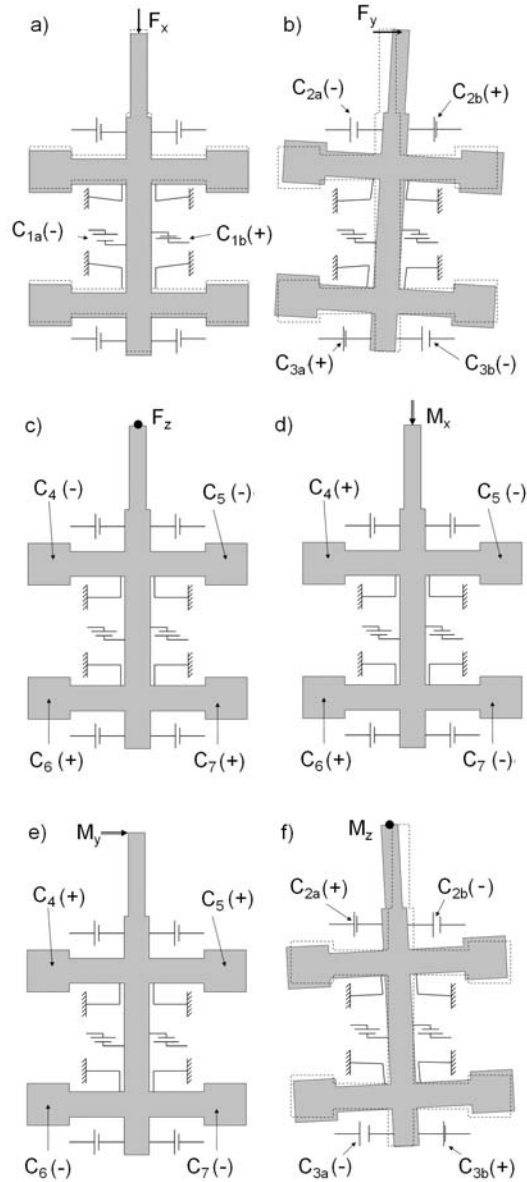

Fig. 4. Capacitance change due to force and torque components applied to the sensor probe.

III. REDUCTION OF NON-LINEARITIES AND CROSSTALK

A number of design optimizations have been performed to reduce non-linearities that would induce errors in the readout signals. These design optimizations also reduce the crosstalk between the individual readout signals.

One unwanted effect is that the x-capacitor pair C_1 and y-capacitors C_2, C_3 are also sensitive to deflections in z-direction since the overlapping area of the parallel plate capacitors changes. To reduce this effect a device layer of 100µm thickness was chosen. The deflections are as large as 2.5µm over the full range of the force sensor. Due to the large device layer thickness, the error due to deflections in the z-axis is less than 2.5%. Additionally, this 2.5% is further reduced by the differential capacitance measurement of the comb drives. Similarly, a displacement in the xy-plane should not influence by the z-axis capacitors (C4,… C7). This has been realized by designing the lower capacitor electrode smaller than the upper one, as shown in Fig. 3b.

To reduce the crosstalk between x-capacitors and y-capacitors the comb drives have been designed such that a lateral deflection does not change the overlapping area of the parallel plate capacitors as shown in Fig. 3a.

Another source of error is that a rotation of the movable body also induces a rotation of the capacitor plates. To reduce this error, the device has been designed such that the maximum rotation angle is only 0.07°. The maximum error occurs in the z-axis capacitors with a length of 1000µm at a deflection of 2.5µm (maximum deflection for the linear range of the sensor). The maximum error calculated is 2.0%.

IV. FABRICATION

In [6], a bulk silicon fabrication process based on a silicon-on-insulator (SOI) wafer is described. This fabrication process is suitable for force sensor designs capable of measuring forces in the x-axis and y-axis only, since all capacitors are perpendicular to the wafer plane. In [16] a fabrication process is described that overcomes this problem by forming additional capacitors parallel to the wafer plane. A combination of the processes in [6] and [16] is presented here, since deflections in all directions must be measured by a transverse capacitor configuration. Additionally, overhanging structures (sensor probe) are required to allow a simple application of the force and torque to the sensor. Fig. 5 displays a cross-section of the sensor for the individual fabrication steps.

a) As a substrate a 100mm diameter silicon wafer is used with a layer of thermal oxide (SiO_2). The thickness of the wafer is 400µm and the thickness of the oxide layer is 1µm.

b) The oxide is removed on the backside of the wafer using reactive ion etching (RIE). Alignment marks are etched into the wafer using deep reactive ion etching (DRIE).

c) A 250nm thick layer of gold is evaporated onto the oxidized topside of the wafer. The metal is etched to

form the lower electrodes and bonding pads.

d) A 5.8μm layer of Benzocyclobutene (Cyclotene 3022-57) is dispensed onto the wafer. The BCB layer is used as adhesive material for low temperature bonding and as a spacer between the device layer and the lower electrodes. The BCB is cured on a hotplate for 35min at a temperature of 200°C in a N_2 atmosphere. After this treatment the BCB is about 60% cured and can resist further processing.

e) A 10μm layer of photoresist is dispensed on the BCB. Subsequently, the BCB is patterned using dry etching. A mixture of O_2 and CF_4 is used for etching the BCB. The remaining photoresist is stripped in acetone.

f) A 100μm thick silicon wafer is bonded onto the lower wafer using adhesive bonding [16]. The wafer is highly doped such that the resistivity is lower than 0.01Ohmcm.

g) A border around the devices is etched into the lower wafer using DRIE. The SiO_2 acts as an etch stop. The SiO_2 is etched using RIE.

h) Pads for making electrical contact to the top wafer are evaporated and patterned as described in step c).

i) The wafer is mounted on a carrier wafer and the topside is etched using DRIE. This step creates the comb drives, the upper electrodes and the springs. A high aspect ratio of 1:20 has been achieved. After etching through the 100μm top wafer the movable structures as well as the whole sensor are automatically released.

j) The MEMS sensor is directly glued and wire-bonded to the PCB of the readout electronics. Holes in the device layer allow bonding to the lower pads.

Since the process allows for the fabrication of electrodes in the x-, y- and z-directions it is not limited to force sensors. Other devices such as multi-axis inertial sensors or multi-axis actuators can also be fabricated using this process.

V. READOUT ELECTRONICS

The capacitance is converted into an analog voltage signal by the MS3110 ASIC. Subsequently, the voltage signal is converted into a digital signal and stored on a PC using a NI USB-6009 data acquisition card. Ideally the readout ASIC is placed as close as possible to the MEMS device for optimal performance. The output voltage V is proportional to the capacitance difference of the capacitor pair C_a and C_b. For small deflections V is proportional to the deflection of capacitor plates as described in detail in [15]. The transfer function for the capacitor pairs C_1, C_2 and C_3 is given by

$$V_{C1} \propto Gain \frac{C_{1a} - C_{1b}}{C_F}, \cdots, V_{C3} \propto Gain \frac{C_{3a} - C_{3b}}{C_F} \qquad (2)$$

where *Gain* and C_F are programmable variables on the ASIC. For the z-axis capacitors C_4-C_7 a reference capacitor C_{ref} soldered onto the printed circuit board (PCB) of the readout electronics is used to enable a differential readout. The output voltage is given by

$$V_{C4} \propto Gain \frac{C_4 - C_{ref}}{C_F}, \cdots, V_{C6} \propto Gain \frac{C_6 - C_{ref}}{C_F}. \qquad (3)$$

The z-capacitors do not create a linear relationship between deflection and output voltage. Therefore, the z-capacitor sensor signal is linearized by the PC after A/D conversion. The MS3110 ASIC can only be used to measure a single capacitor pair at one time. For the experiments described in this work the capacitors have been read out sequentially by multiplexing.
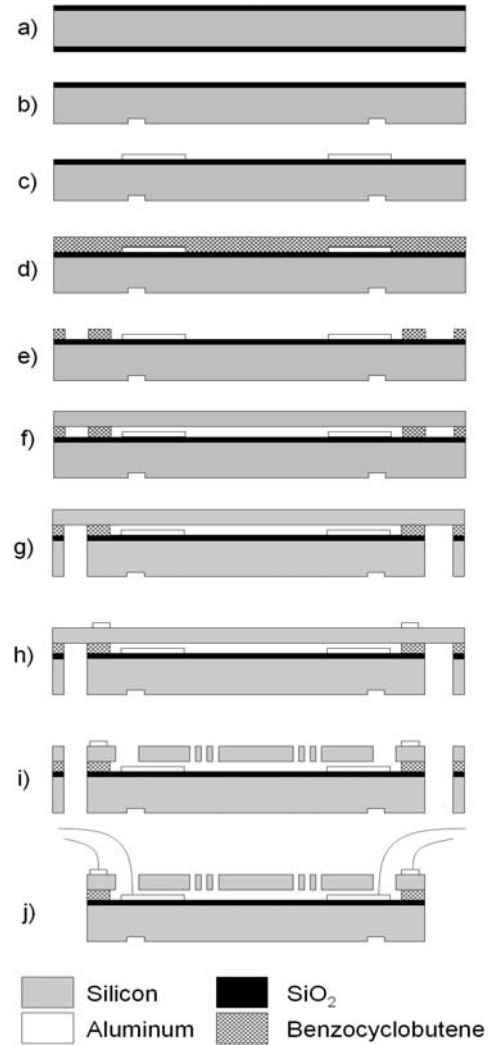

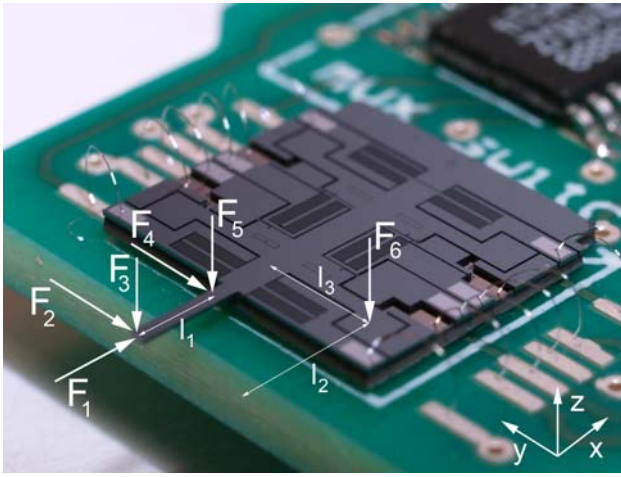Fig.5. Microfabrication process steps

Fig.6. Reference force vectors

calibration matrix $\underline{\underline{A}}$ is given by

$$\underline{\underline{A}} = 1000 \cdot \begin{bmatrix} 6.849 & -0.315 & -0.137 & 0.152 & 0.263 & 0.128 & 0.122 \\ 0.168 & 2.216 & 1.235 & 0.020 & 0.000 & 0.017 & 0.005 \\ 0.016 & -0.100 & -0.304 & -2.692 & 1.519 & 0.218 & 0.686 \\ -0.161 & -0.140 & -0.0262 & -3.361 & 1.611 & -7.994 & 1.381 \\ -0.151 & 0.0754 & 1.870 & 10.94 & -12.22 & 5.223 & -1.273 \\ 0.500 & 7.076 & 9.746 & -0.286 & 0.232 & 0.418 & 0.853 \end{bmatrix} \quad (5)$$

for forces given in μN and torques in nNm. The matrix has full rank indicating that a decomposition of the force and torque components can be performed. The condition number of $\underline{\underline{A}}$ is 19.34. The precision of the calibration matrix strongly depends on the accurate application of the reference force vectors. The calibration procedure has been repeated four times to reduce errors.
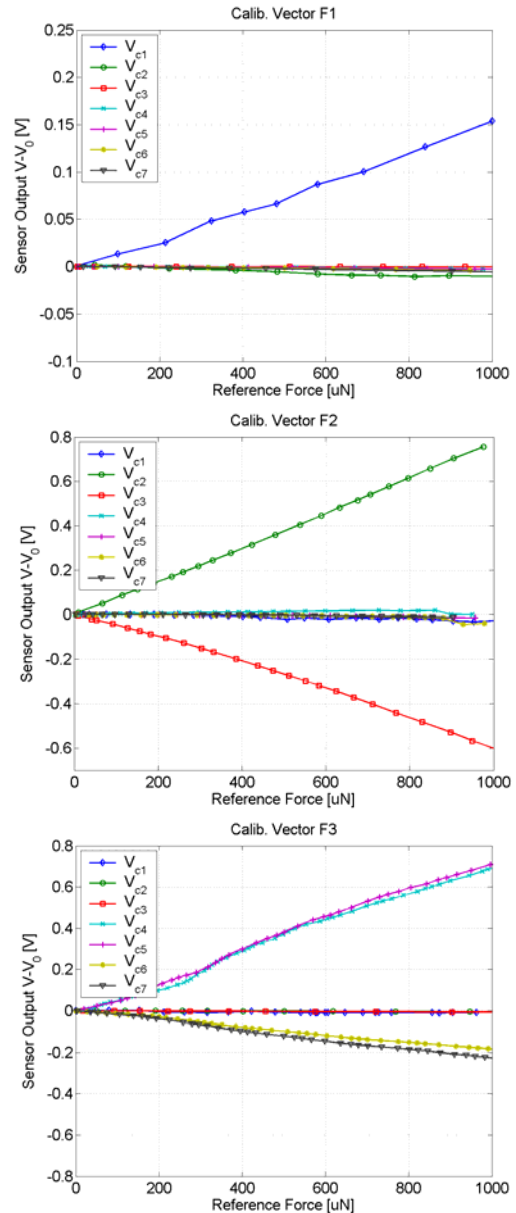
VI. CALIBRATION

The calibration of multi-axis MEMS force sensors is difficult for several reasons, including the need to apply known force vectors at precise positions and orientations and risk damaging the small and fragile microdevices [18,19]. The goal of the calibration is to obtain the components of the calibration matrix $\underline{\underline{A}}$, which characterizes the linear relationship between the seven analog sensor output signals $\underline{V}=[V_{c1}, V_{c2},..., V_{c7}]^T$ and the loads $\underline{F}=[F_x, F_y, F_z, M_x M_y, M_z]^T$ applied to the sensor.

$$\begin{bmatrix} F_x \\ F_y \\ F_z \\ M_x \\ M_y \\ M_z \end{bmatrix} = \underline{\underline{A}}^{6x7} \cdot \begin{bmatrix} V_{C1} \\ V_{C2} \\ V_{C3} \\ V_{C4} \\ V_{C5} \\ V_{C6} \\ V_{C7} \end{bmatrix} \qquad \underline{\underline{A}} = \begin{bmatrix} a_{11} & a_{12} & ... & a_{17} \\ a_{21} & a_{22} & ... & a_{27} \\ ... & ... & ... & ... \\ a_{61} & a_{62} & ... & a_{67} \end{bmatrix} \quad (4)$$

For the calibration of the six-axis force-torque sensors a commercial single-axis reference force sensor (FemtoTools FT-S270) is used. The six-axis sensor is mounted on a 3-axis micromanipulator (Sutter MP285) and the reference sensor is attached onto a three-axis rotation stage. This setup enables the accurate application of known reference force vectors at multiple locations and directions. Six reference forces at different orientations and positions are chosen $F_1, ..., F_6$ as shown in Fig. 6. The output of all seven capacitors is saved. Fig. 7 and Fig. 8 show the slopes of the seven output signals for the calibration vectors $F_1, ..., F_6$.

The sensor has been calibrated for forces up to 1000μN and torques up to 2600nNm. The standard deviation of the noise level of the capacitive readout corresponds to 1.4 μN and 3.6nNm respectively, at a readout frequency of 30Hz. After collecting the seven output signals for all six calibration vectors the components of the calibration matrix is calculated using a least-square optimization method by MATLAB software. For the given design, a typical

Fig. 7. Output voltage for the applied reference force vectors $F_1,...,F_3$
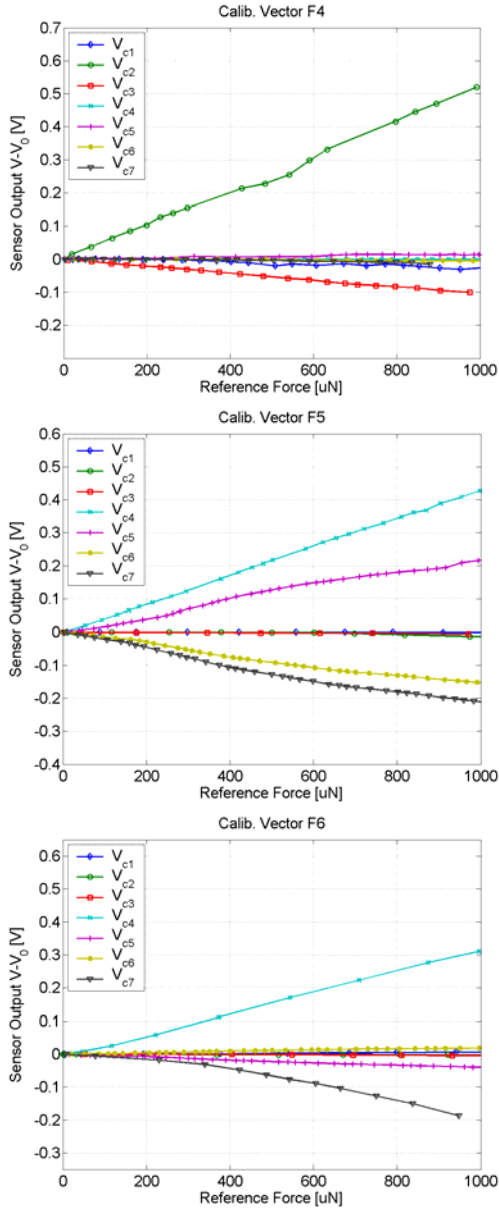
Fig. 8. Output voltage for the applied reference force vectors $F_4,...,F_6$

VII. CONCLUSION

A MEMS six-axis force sensor intended for microrobotic applications such as force controlled microhandling, biomaterial characterization, microsystems characterization and material science has been presented. This is the first six-axis MEMS force-torque sensor that has been successfully designed and fabricated. The chip size of the sensor is 10mm x 9mm x 0.5mm. A 3mm long probe protrudes from the device which simplifies the application of the load onto the sensor. The wafer-level manufacturing process is not limited to force sensors and may be used for other transducers such as multi-axis inertial sensors or multi-axis actuators. The evaluation of the noise level shows that a

resolution in the range of single micro-Newton and nano-Newtonmeter has been achieved, which is three orders of magnitude better than for conventional six-axis force sensors. The six-axis force sensor has been calibrated and the calibration matrix has been computed based on experimental data.

REFERENCES

[1] J. J. Abbott, Z. Nagy, F. Beyeler, B. J. Nelson, "Robotics in the small, Part I: Microrobotics", IEEE Robotics & Automation Magazine," vol. 14, pp. 92-103, 2007.
[2] S. Fahlbusch, S. Fatikow, "Force Sensing in microrobotic systems - an overview," Proc. ICECS, Lisboa, pp. 259-262, 1998.
[3] F. Arai, T. Sugiyama, T. Fukuda, H. Iwata, K. Itoigawa, "Micro tri-axial force sensor for 3D bio-micromanipulation," International Conference on Robotics and Automation, 1999.
[4] F. Arai, D. Ando, T. Fukuda, Y. Nonoda, T. Oota, "Micro manipulation based on micro physics - strategy based on attractive force Reduction and stress measurement," IROS, pp.263-241, 1995.
[5] FemtoTools GmbH, Switzerland
[6] Y. Sun, B. J. Nelson, P. D. Potasek, E. Enikov, "A bulk microfabricated multi-axis capacitive cellular force sensor using transverse comb drives", Journal of Micromechanics and Microengineering, Vol. 12, pp. 832-840, 2002.
[7] X. Zhang, "Silicon microsurgery-force sensor based on diffractive optical MEMS encoders," Sensor Review, vol. 24 pp.37-41, 2004.
[8] S. Bütefisch, S. Büttgenbach, T. Kleine-Besten, U. Brand, "Micromechanical three-axial tactile force sensor for micromaterial characterization," Microsystem Technologies, vol. 7, pp. 171-174, 2001.
[9] T. Mei, W. J. Li, Y. Ge, Y. Chen, L. Ni, M. H. Chan, "An integrated MEMS three-dimensional tactile sensor with large force range," Sensors and Actuators A, vol. 80, pp.155-162, 2000.
[10] P. Valdastri, S. Roccella, L. Beccai, E. Cattin, A. Menciassi, M. C. Carrozza, P. Dario, "Characterization of a novel hybrid silicon three-axial force sensor," Sensors and Actuators A, pp. 249-247, 2005.
[11] A. Sieber, P. Valdastri, K. Houston, A. Menciassi, P. Dario, "Flip chip microassembly of a silicon triaxial force sensor on flexible substrates," Sensors and Actuators A, pp. 421-428, 2008.
[12] J. Brugger, M. Despont, C. Rossel, H. Rothuizen, P. Vettiger, M. Villemin, "Microfabricated ultrasensitive piezoresistive cantilevers for torque magnetometry," Sensors and Actuators A, vol. 73, 235-242, 1999.
[13] F. Beyeler, S. Muntwyler, Z. Nagy, C. Graetzel, M. Moser, B.J. Nelson, "Design and calibration of a MEMS sensor for measuring force and torque acting on a magnetic microrobot," Journal of Micromechanics Microengineering, vol. 18, 2008.
[14] A. Cherry, J. Abadie, E. Piat, "Modelling and optimization of a floating triangular platform used for nano and microforces sensing," IEEE International Conference on robotic and automation, 2007.
[15] Y. Sun, B.J. Nelson, "MEMS capacitive force sensors for cellular and flight biomechanics," Biomedical Materials, vol. 2, pp. 16-22, 2007.
[16] Y. Watanabe, T. Mitsui, T. Mineta, Y. Matsu, K. Okada, "SOI micromachined 5-axis motion sensor using resonant electrostatic drive and non-resonant capacitive detection mode," Sensors and Actuators A, pp. 116-123, 2006.
[17] J. Oberhammer, F. Niklaus, G. Stemme, "Selective wafer-level adhesive bonding with benzocyclobutene for fabrication of cavities," Sensors and Actuators A, vol. 105, 297-304, 2003.
[18] K. Kim, Y. Sun, R. M. Voyles, B. J. Nelson, "Calibration of multi-axis MEMS force sensors using the shape-from-motion method," IEEE Sensors Journal, vol. 7 pp. 344-51, 2007.
[19] W. Jin, C. D. Mote Jr., "On the calibration of Multicomponent Microforce Sensors", Journal of Microelectromechanical Systems, Vol. 7, No. 2, June 1998.